Screening and retardation effects on 180°-domain wall motion in ferroelectrics: Wall velocity and nonlinear dynamics due to polarization-screening charge interactions

E. A. Eliseev
Institute for Problems of Materials Science, National Academy of Sciences of Ukraine, 3 Krjijanovskogo, 03142 Kiev, Ukraine

A. N. Morozovska* and G. S. Svechnikov
Institute of Semiconductor Physics, National Academy of Sciences of Ukraine, 41 pr. Nauki, 03028 Kiev, Ukraine

E. L. Rumyantsev, E. I. Shishkin, and V. Y. Shur
Institute of Physics and Applied Mathematics, Ural State University, Ekaterinburg 620083, Russia

S. V. Kalinin†
The Center for Nanophase Materials Sciences and Materials Science and Technology Division, Oak Ridge National Laboratory, Oak Ridge, Tennessee 37831, USA

(Received 7 September 2008; revised manuscript received 7 November 2008; published 8 December 2008)

The effect of the domain wall intrinsic width, relaxation time of the screening charges, and the dead layer thickness on the velocity of the planar 180°-domain wall moving under homogeneous external electric field in ferroelectric capacitor is analyzed. The limiting cases of domain wall motion, including (i) the motion induced by the external and local internal field originated at the wall-surface junction for nonzero dead layer thickness and (ii) the motion induced by the effective electric field averaged over the domain wall surface, are considered. We demonstrate the crossover between two screening regimes: the first one corresponds to the low domain wall velocity, when the wall drags the sluggish screening charges, while the second regime appears for high domain wall velocity, when the delay of sluggish screening charges are essential and the wall depolarization field is screened by the instant free charges located at the electrode. The integral and approximate analytical expressions for electric field and algebraic equation for the domain wall velocity are derived. It is shown that in the local-field limit the motion can be unstable, since the internal field at the wall-surface junction decreases for larger domain wall velocities, making possible self-acceleration of the wall near the top surface. The instability may lead to the domain wall-surface bending and actual broadening in thick samples, as well as formation of periodic domain structures in the direction of wall motion. The motion in the limit of the averaged effective field is always stable.

DOI: 10.1103/PhysRevB.78.245409 PACS number(s): 77.80.Fm, 77.22.Ej

I. INTRODUCTION

Domain wall (DW) motion in ferroelectric and ferromagnetic materials is one of the critical factors in determining the functionality of ferroic devices, including the ultimate switching speed, uniformity of switching behavior, and stability of domain patterns in periodic fields. In the ideal bulk materials, the wall motion mechanisms are governed by the wall-lattice interactions as studied in detail by Vanderbilt.[1] The relationship between the lattice pinning and wall velocity has been addressed in great detail starting from the pioneering work by Muller and Weinreich[2] until recent advances by density-functional theory.[3] The presence of bulk disorder due to the random-bond and random-field defects coupling to order parameter and thermal excitations gives rise to a broad spectrum of remarkable physical phenomena including transitions between pinned, creep, and sliding regimes, dynamic phase transitions, and self-organized criticalities.[4–6] In this case, the domain wall dynamics is assumed to be effectively local and controlled only by the driving force and disorder rather than interface and boundary conditions.

However, it is well known that properties of ferroelectric materials are ultimately sensitive to the boundary conditions on surfaces and interfaces that define the depolarization fields inside the materials. Recently Qiu *et al.*[7] developed methodology that accounts for electrostatic boundary conditions, the formation of misfit dislocations, and polydomain structures, which produces the strain-thickness diagram of phase stability in epitaxial $PbTiO_3$ ultrathin ferroelectric films. These nonlocal effects define stability of ferroelectric phase and were predicted to trigger transitions to spatially modulated and toroidal phases[8,9] in rigid ferroelectric materials. In realistic materials, the depolarization energy affects the stability of materials with respect to charge species adsorption,[10–12] formation of surface charge layers,[13,14] or oxygen vacancy formation[15] that provide efficient screening mechanisms on free surfaces. In capacitor structures, the formation of layers with reduced ferroelectric properties[16] and propagation of ferroelectric distortion through the interfaces[17–19] have been reported. However, these theoretical studies address mainly *static* properties of ferroelectric materials as controlled by nonlocal depolarization field effects.

To complement the static studies, many experimental and theoretical studies report the broad spectrum of dynamic nonequilibrium phenomena at high domain wall velocities, including domain nucleation in front of the moving domain wall.[20,21] The effect of domain-domain electrostatic interac-

tion leads to the effect of correlated nucleation, which in turn results in the formation of the self-assembled structures.[22] Various manifestations of the effect are the most pronounced for ineffective screening of depolarization fields.[23,24] It has been demonstrated experimentally that two-dimensional (2D) and one-dimensional (1D) growth of ensembles consist of isolated nanodomains.[25] These results illustrate the importance of depolarization effects on the kinetics of the domain structure formation and open new abilities of submicron domain and nanodomain engineering, which is rapidly developed nowadays.[26] However, despite the rapidly expanding experimental knowledge in this area, very few theoretical works address the dynamic phenomena during domain wall motion mediated by depolarization field and switching charge dynamics. This lack of knowledge is particularly important in the case of ferroelectric capacitors, in which domain wall motion is available for experimental studies only in limited cases.

It is generally believed that domain dynamics in capacitor will be strongly affected by the presence of a thin layer at the interface between ferroelectric and electrode responsible for the difference between the field seen by the domain wall and the applied field. For instance, the presence of misfit dislocations on the boundary between epitaxial ferroelectric film and its substrate or electrode—confirmed experimentally—should lead to the appearance of dead layer with degraded polar properties as clearly demonstrated experimentally and theoretically by Dittmann *et al.*,[27] Misirlioglu *et al.*,[28] Alpay *et al.*,[29] and Nagarajan *et al.*[30] Actually, the authors showed that variations in the strain elastic field around the dislocation core lead to localized polarization gradients, which in turn produce strong depolarizing stray fields resulting into suppression of ferroelectricity in the vicinity of a dislocation. For periodic misfit dislocations the depth of stray field decay was about ~10 nm. As discussed in Refs. 28–30, the interface defects such as arrays of misfit dislocations inevitably appear at the film surfaces and form dead layers of tens of nanometers thick due to the strain-induced strong stray electric fields. The appearance of such ultrathin "intrinsic" dead layers at the ferroelectric surfaces seems almost inevitable effect. Naturally, artificially introduced or aged dead layers may be much thicker.[23,24] For instance, Grossmann *et al.*[31] attributed the experimentally observed dielectric constant decrease in ferroelectric thin films of $Pb(Zr,Ti)O_3$ by the growth of a thin surface layer with suppressed ferroelectric properties in the course of aging.

The earliest theoretical models for dead layers were proposed by Merz,[32] Drougard and Landauer,[33] and Callaby.[34,35] The Merz's model contains a nearby-electrode layer with the dielectric permittivity which is much smaller than that in the bulk but which, however, can be switched like the bulk of the ferroelectric. The surface layer in the model of Drougard and Landauer[33] is nonswitchable, has a low dielectric permittivity, and exhibits an appreciable conduction. In the model of Callaby, the material of the capacitor is homogeneous in all the properties except the wall mobility, which is assumed to be much smaller inside the surface layer. In all analyses to date, the domain wall was assumed to be infinitely thin, leading to unphysical singularities in electrical and elastic fields at the surfaces and interfaces and precluding the development of deterministic mesoscopic models that account for polarization nonlinearity and field distribution within the wall. Later on, Grossmann *et al.*[36] theoretically discussed the interface screening model in order to explain imprint in ferroelectric thin films of $Pb(Zr,Ti)O_3$ by a large electric field within a surface layer with deteriorated ferroelectric properties. Pintilie and Alexe[37] proposed the model for metal-ferroelectric-metal heterostructures with Schottky contacts that introduced the ferroelectric polarization as a sheet of surface charge located at a finite distance from the electrode interface. Recently Misirlioglu *et al.*[38] theoretically considered the impact of nonferroelectric layer and interface charge on the dielectric properties of the ferroelectric film, for instance, the apparent enhancement of polarization were revealed in $PbTiO_3$ films with layer of $SrTiO_3$.

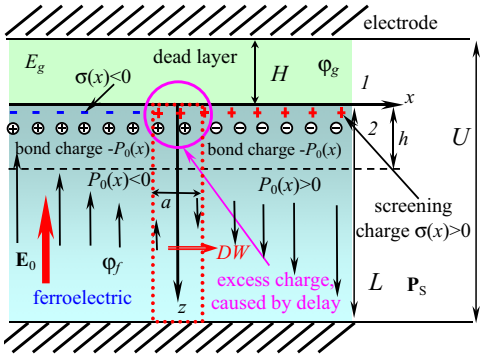

FIG. 1. (Color online) Capacitor geometry. $\mathbf{P}_0(x,z,t)$ is spontaneous polarization, $\mathbf{E}_f$ is electric field *inside the ferroelectric*, and voltage U is applied between the electrodes. Screening charge layer, which originated from bend bending, is localized inside ferroelectric near the dead layer boundary. Dotted line indicates the moving boundary of 180°-domain wall. The normal vector $\mathbf{n}$ is pointed from media 1 to media 2

Here, we consider the effect of intrinsic wall width, relaxation time of the screening charge, and the dead layer thickness on the velocity of the planar 180°-domain wall uniformly moving under homogeneous external field in ferroelectric capacitor. The wall dynamics is analyzed within the full Ginzburg-Landau model, thus providing insight into mesoscopic structure of moving domain wall. Special attention is paid to the effects of depolarization electric field induced by the bound charge at the wall-surface junction near the dead layer.

II. PROBLEM STATEMENT

The schematic representation of ferroelectric capacitor with an interfacial layer is shown in Fig. 1 and consists of (1) conducting top and bottom electrodes, (2) wide-band-gap semiconductor ferroelectric film (f) of thickness L with dielectric permittivity tensor $\hat{\varepsilon}_{ij}^{f}$ (Ref. 39) and upper space-charge layer with time and coordinate-dependent surface charge density $\sigma(x,t)$ that may partially screen the spontaneous polarization outside the film, and (3) deposited dead layer (g) of thickness H with isotropic dielectric permittivity ε_g (perfect insulator).

Note that due to the effects of "reflections" in bottom electrode this asymmetric system is equivalent to symmetric capacitor with two dead and screening charge layers and thickness of ferroelectric doubled.[40] In this description, it is implicitly assumed that the conductivities of the electron and hole are comparable.

Equations of state relate electrical displacement $\mathbf{D}$ and electric field $\mathbf{E}$ as

$$\mathbf{D}_g = \varepsilon_0 \varepsilon_g \mathbf{E}_g, \tag{1}$$

$$\mathbf{D}_f = \varepsilon_0 \mathbf{E}_f + \mathbf{P} \approx \varepsilon_0 \hat{\varepsilon}^f_{ij} \mathbf{E}_f + \mathbf{P}_0(x,t). \tag{2}$$

Here $\mathbf{P}(x,z,t)$ is polarization vector, $\mathbf{P}_0(x,t)=[0,0,\mathrm{P}_0(x,t)]$ is spontaneous polarization vector pointed either along or opposite the polar axis z and depending on coordinate x, and time t with respect to the domain wall motion. For chosen geometry div $\mathbf{P}_0(x,t)=0$ inside ferroelectric.

Electrostatic quasistationary Maxwell equation rot $\mathbf{E}=0$ should be satisfied for each layer. Below we introduce the potential φ of quasistationary electric field $\mathbf{E}_{g,f}(x,z,t) = -\nabla \varphi_{g,f}(x,z,t)$. Inside the dead layer and outside the screening layer potential φ satisfies the Laplace's equation. Thus, Maxwell's equation div $\mathbf{D}=0$ along with condition div $\mathbf{P}_0 = 0$ and Eqs. (1) and (2) lead to

$$\left(\frac{\partial^2}{\partial z^2} + \frac{\partial^2}{\partial x^2} \right) \varphi_g = 0, \quad \text{for} \quad -H < z < 0, \tag{3}$$

$$\varepsilon_0 \left(\varepsilon^f_{33} \frac{\partial^2}{\partial z^2} + \varepsilon^f_{11} \frac{\partial^2}{\partial x^2} \right) \varphi_f = 0, \quad \text{for} \quad 0 < z < L. \tag{4}$$

Equations (3) and (4) are supplemented with the boundary conditions of fixed top and bottom electrode potentials and continuous potential and normal component (n) of displacement on the boundaries between dead layer and ferroelectric, namely,

$$\varphi_g(z=-H)=0, \quad \varphi_g(z=0)=\varphi_f(z=0), \quad \varphi_f(z=L)=U, \tag{5}$$

$$D_{fn} - D_{gn} = -\varepsilon^f_{33} \frac{\partial \varphi_f(x,z=0)}{\partial z} + \frac{P_{0n}(x,t)}{\varepsilon_0} + \varepsilon_g \frac{\partial \varphi_g(x,z=0)}{\partial z} = \sigma(x,t), \tag{6}$$

where $\sigma(x,t)$ is the density of the free screening surface charge.

Here we consider the case of the uniformly moving 180° domain wall, in which case the wall shape is invariant in space. This approximation is justified given that shape fluctuations in the z directions are associated with significant depolarization fields.[41] The fluctuations in the longitudinal direction and front stability will be addressed elsewhere.

In this 1D approximation for the z component of polarization profile is

$$P_0(x,t) \approx P_0(x - vt). \tag{7}$$

The unknown domain wall velocity v should be found self-consistently. The relaxation equation for effective surface charge density σ is derived in the Appendix Sec. 1 as

$$\tau \frac{\partial \sigma(x,t)}{\partial t} = P_0(x - vt) - \sigma(x,t), \tag{8}$$

where the relaxation time $\tau = \varepsilon_0 \varepsilon^f_{11}/\lambda$, and λ is the electric conductivity of the ultrathin screening layer.

III. SOLUTION FOR THE SCREENING CHARGE AND ELECTRIC FIELD

Under the condition of full screening $\sigma(x,0)=P_0(x)$ at the initial moment of time $t=0$, solution of Eq. (8) is

$$\sigma(x,t) = \exp\left(-\frac{t}{\tau}\right) \left[P_0(x) + \int_0^t \frac{dt'}{\tau} P_0(x - vt') \exp\left(\frac{t'}{\tau}\right) \right]. \tag{9}$$

This expression can be rewritten as follows:

$$\sigma(x,t) = P_0(x - vt) + v \int_0^t dt' \frac{\partial P_0(x - vt')}{\partial x} \exp\left(-\frac{t - t'}{\tau_m}\right). \tag{10}$$

Hereinafter the following approximations for the polarization distribution within the domains wall will be used:

$$P_0(x) = P_S \begin{cases} 1 - \exp\left(-\dfrac{x}{a}\right), & x > 0 \\ -1 + \exp\left(\dfrac{x}{a}\right), & x < 0. \end{cases} \tag{11}$$

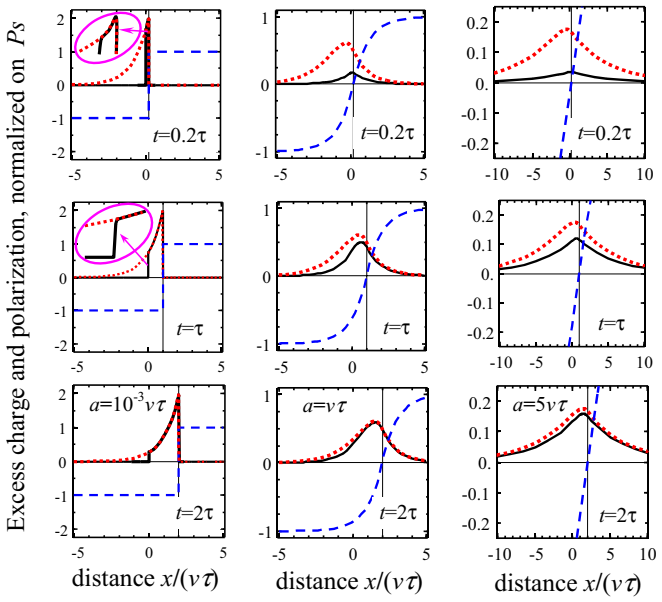

FIG. 2. (Color online) Solid curves are exact distribution of the excess charge $\delta\sigma(x,t)$ calculated from Eq. (12), dotted curves are approximate distribution of $\delta\sigma(x,t)$ calculated from Eq. (13), dashed curves are the polarization distribution $P_0(x-vt)$ at different moments of time $t/\tau=0.2$, 1, 2 (from the top to the bottom) for $(a/v\tau)=10^{-3}$ (first row), $(a/v\tau)=1$ (second row), and $(a/v\tau)=5$ (third row).

Here a is the effective half width of the domain wall, e.g., 0.5–2 nm. Here, P_S is spontaneous polarization. Note that polarization distribution (11) is continuous at $x=0$ along with the first derivative $P_0'(x)=\exp(-|x|/a)P_S/a$.

Substitution of Eq. (11) into Eq. (10) gives the following analytical expression for the excess charge $\delta\sigma(x,t)=\sigma(x,t)-P_0(x-v\,t)$:

$$\delta\sigma(x,t)=P_S\begin{cases}\dfrac{v\tau}{a+v\tau}\left[\exp\left(-\dfrac{x-vt}{a}\right)-\exp\left(-\dfrac{x}{a}-\dfrac{t}{\tau}\right)\right] & \text{for } x>vt\\ \dfrac{v\tau}{a-v\tau}\left[\exp\left(\dfrac{x-vt}{a}\right)-\exp\left(\dfrac{x-vt}{v\tau}\right)\right]+\dfrac{v\tau}{a+v\tau}\left[\exp\left(\dfrac{x-vt}{v\tau}\right)-\exp\left(-\dfrac{x}{a}-\dfrac{t}{\tau}\right)\right] & \text{for } 0<x<vt\\ \dfrac{v\tau}{a-v\tau}\left[\exp\left(\dfrac{x-vt}{a}\right)-\exp\left(\dfrac{x}{a}-\dfrac{t}{\tau}\right)\right] & \text{for } x<0.\end{cases} \tag{12}$$

Excess charge, i.e., the difference of surface free charge and bond charge $\delta\sigma(x,t)=\sigma(x,t)-P_0(x-vt)$, is caused by the delay in screening. For the very slow moving wall ($\tau v\to 0$) excess charge is absent.

Under the condition $t\gg\tau$, i.e., in the stationary regime, the expression for the surface charge density is derived from Eq. (12) as

$$\sigma(x,t)\approx P_0(x-vt)+P_S\begin{cases}\dfrac{v\tau}{a+v\tau}\exp\left(-\dfrac{x-vt}{a}\right), & x>vt\\ \dfrac{v\tau}{a-v\tau}\left[\exp\left(\dfrac{x-vt}{a}\right)-\dfrac{2v\tau}{a+v\tau}\exp\left(\dfrac{x-vt}{v\tau}\right)\right], & x<vt.\end{cases} \tag{13}$$

The accuracy of solution (13) is clear from Fig. 2. In this approximation, charge density $\delta\sigma(x,t)$ depends only on $x-vt$, i.e., describes the charge wave accompanying moving domain wall at times $t\gg\tau$. In the limiting case of ultrathin (or rapidly moving) domain wall $(a/v\tau)\ll 1$, approximation (13) works with high accuracy at distances $x>vt-a$ (i.e., in front of the domain wall) even starting from the small times $t\ll\tau$ (see the first row in Fig. 2). The spatial dependence of $\delta\sigma(x,t)$ is jumplike as anticipated for $(a/v\tau)\to 0$.

In the limiting case of thick (or slow moving) domain walls, $(a/v\tau)\geq 1$, approximation (13) works with satisfactory accuracy only at $t\gg\tau$ (see the last rows in Fig. 2). Reasonable estimations for the domain wall intrinsic width $a=5-0.5$ nm, velocity $v=10^{-6}-10^{-3}$ m/s, and relaxation time $\tau=10^{-3}-1$ s lead to the interval $(a/v\tau)=1-10^{-6}$, justifying the limit of $(a/v\tau)\ll 1$. Thus, below we use approximation (13) in the region $x>vt-a$.

The distinctive feature of the analytical solutions (12) and (13) is, in fact, that the maximum of screening charge is located behind the moving wall at finite width a and exactly at the wall in the case $a\to 0$. Hence, the screening charge effect on domain wall dynamics can be described only in the case of finite wall width.

The normal component of the electric field inside the ferroelectric layer has the form (Appendix Sec. 1),

$$E_{f3}(x,z,t)=E_{d3}(x,z,t)+E_0,\quad E_0=-\frac{U\varepsilon_g}{H\varepsilon_{33}^f+L\varepsilon_g}, \tag{14a}$$

$$E_{d3}(x,z,t)\approx-\int_{-\infty}^{+\infty}dk\frac{\exp(-ikx)}{\varepsilon_0\sqrt{2\pi}}\times\frac{[\tilde{P}_0(k,t)-\tilde{\sigma}(k,t)]\tanh(kH)\cosh[k(L-z)/\gamma]}{\varepsilon_{33}^f\cosh(kL/\gamma)\tanh(kH)+\gamma\varepsilon_g\sinh(kL/\gamma)}. \tag{14b}$$

Here $\gamma=\sqrt{\varepsilon_{33}^f/\varepsilon_{11}^f}$ is the dielectric anisotropy factor. $\tilde{P}_0(k,t)$ and $\tilde{\sigma}(k,t)$ are Fourier images of $P_0(x,t)$ and $\sigma(x,t)$ over coordinate x. The term $E_{d3}(x,z,t)$ in Eq. (14a) is the internal electric field produced by the wall and partially screened by the free charges on the top electrode. Complete screening is achieved for $H=0$; also the screening is realized by the surface screening charges $\sigma(x,t)$ with delay deter-

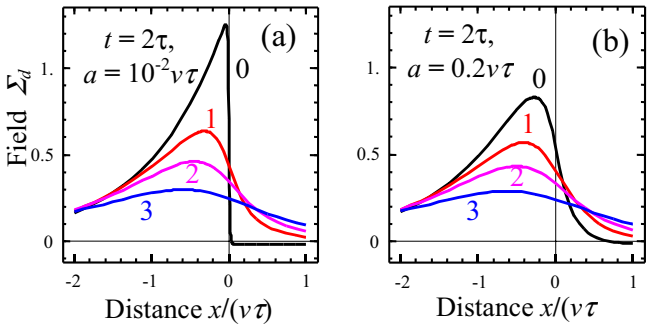

FIG. 3. (Color online) The dependence of the normalized internal field $\Sigma_d=\varepsilon_0\varepsilon_{33}^f E_{dm}/P_S$ via the distance $x/v\tau$ for parameters $\gamma\varepsilon_g/\varepsilon_{33}^f=0.5$, $(H/v\tau)=10$, $L/(\gamma v\tau)=100$ and (a) $(a/v\tau)=10^{-2}$, and (b) $(a/v\tau)=0.2$. Curves 0–3 correspond to the different depth z: $z/(\gamma v\tau)=0$, 0.25, 0.5, and 1.

mined by finite relaxation time τ. The last term in Eq. (14a) is the external electric field induced by applied bias U. Note that far from the wall $E_{d3} \to \frac{\sigma - P_S}{\varepsilon_0} \frac{H}{H\varepsilon_{33}^f + L\varepsilon_g}$ as anticipated for the stationary case.

The x distribution of the depolarization field is shown in Fig. 3 for different depths z. It is clear that the field $E_{d3}(x,z,t)$ is maximal behind the moving wall for finite intrinsic width a and achieves maximum exactly at the wall in the limiting case $a \to 0$ (corresponding to the jump at the wall). The field maximum decreases and diffuses with increasing penetration depth z.

Using expression (13) the Fourier image of $\delta\sigma(x,t)$ was found as

$$\delta\tilde{\sigma}(k,t) = P_S \sqrt{\frac{2}{\pi}} \frac{v\tau \exp(ikv\tau)}{(1+a^2k^2)(1+ikv\tau)}. \tag{15}$$

From Eq. (15) the integral representation of the field in any point of the system can be obtained in a straightforward manner. However, given our interest of the influence of delayed screening on the velocity of domain wall, below we concentrate on the depolarization field value at the domain wall surface $E_{d3}(x=vt,z) \equiv E_{\mathrm{dm}}(z)$. Simple transformation of Eqs. (14b) and (15) allows the field at the domain wall-surface junction to be obtained as

$$E_{\mathrm{dm}}(z) = \frac{2}{\pi}\frac{P_S}{\varepsilon_0}\int_0^\infty \frac{dk \cdot v\tau \tanh(kH)\cosh[k(L-z)/\gamma]}{(1+a^2k^2)[1+(kv\tau)^2][\varepsilon_{33}^f \cosh(kL/\gamma)\tanh(kH) + \gamma\varepsilon_g \sinh(kL/\gamma)]}. \tag{16}$$

For the case of either small external field of thin films, when the length of the nascent step nucleus on the moving wall either is rather large (as inversely proportional to external field) (Ref. 2) or approaches film thickness, we consider the depolarization field energy excess averaged on the domain wall surface. This could be approximated by the depolarization field given by Eq. (16) averaged along the domain wall surface as

$$\langle E_{\mathrm{dm}}(z)\rangle = \frac{2}{\pi}\frac{P_S}{\varepsilon_0}\int_0^\infty \frac{dk \cdot v\tau \tanh(kH)\tanh(kL/\gamma)(\gamma/kL)}{(1+a^2k^2)[1+(kv\tau)^2][\varepsilon_{33}^f \tanh(kH) + \gamma\varepsilon_g \tanh(kL/\gamma)]}. \tag{17}$$

From this analysis, the effect of depolarization field on domain velocity v can be found. Below we consider the two limiting cases, when the velocity of the wall is determined by the nucleation rate either at the wall-surface junction (i) or over the entire wall surface (ii).[33] Using linear approximation we suppose that wall velocity dependence on the electric field is

$$\nu = \begin{cases} 0, & E < E_{\mathrm{th}} \\ \mu[E(v) - E_{\mathrm{th}}], & E > E_{\mathrm{th}}, \end{cases} \tag{18}$$

where μ is the wall mobility and E_{th} is the threshold value of electric field, E is the sum of external filed E_0 and depolarization field E_{dm}, namely, $E(v)=E_0+E_{\mathrm{dm}}(0)$ for the case (i), while $E(v)=E_0+\langle E_{\mathrm{dm}}(z)\rangle$ for the case (ii). The dependence of E_{dm} on the wall velocity v can be found from Eqs. (16) and (17).

IV. ELECTRIC FIELD AT THE WALL-SURFACE JUNCTION

For the case of either thick films ($L \gg H$) or for high external field (when the nucleus is small), the influence of the bottom electrode in Eq. (16) can be neglected to yield the following expression for the depolarization field at wall-surface junction:

$$E_{\mathrm{dm}}(0) = \frac{P_S}{\varepsilon_0}\frac{2}{\pi}\int_0^\infty \frac{v\tau dk}{(1+a^2k^2)[1+(kv\tau)^2]} \times \frac{\sinh(kH)}{\varepsilon_{33}^f \sinh(kH) + \gamma\varepsilon_g \cosh(kH)}. \tag{19}$$

It should be noted that the inequality $L \gg H$ allows us to regard external field E_0 independent on the dead layer thickness H and permittivity ε_g and approximately equal to U/L in accordance with Eq. (14a).

The integral representation (19) can be reduced to the series over charges and their images in the top electrode

$$E_{\mathrm{dm}} = \frac{P_S}{\varepsilon_0(\varepsilon_{33}^f + \gamma\varepsilon_g)}\frac{v\tau}{a+v\tau}\left(1 - \sum_{n=1}^{\infty}\frac{2\gamma\varepsilon_g(\varepsilon_{33}^f - \gamma\varepsilon_g)^{n-1}}{(\varepsilon_{33}^f + \gamma\varepsilon_g)^n} \times \frac{v\tau F(2nH, v\tau) - aF(2nH,a)}{v\tau - a}\right), \tag{20a}$$

where the following transcendental function:

$$F(z,a) = \frac{2}{\pi}\int_0^\infty dk \frac{a\exp(-kz)}{[1+(ka)^2]} \approx \frac{2a}{2a+\pi z} \tag{20b}$$

is introduced. The infinite number of images is related to multiple reflections in the top electrode and the interface

between ferroelectric and dead layers. Also it should be noted that series (20) is much more convenient for numerical calculation than integral representation (19).

Using integral (19) and series (20), we derived the following expressions for $E_{\rm dm}$ for two limiting cases corresponding to the high and small values of dead layer thickness H:

$$E_{\rm dm} = \begin{cases} \dfrac{P_S}{\varepsilon_0(\varepsilon_{33}^f + \gamma\varepsilon_g)} \dfrac{v\tau}{a + v\tau}\left[1 - \dfrac{2\gamma\varepsilon_g}{\pi(\varepsilon_{33}^f - \gamma\varepsilon_g)} \ln\left(\dfrac{\varepsilon_{33}^f + \gamma\varepsilon_g}{2\gamma\varepsilon_g}\right)\dfrac{a + v\tau}{H}\right], & H \gg \{a, v\tau\} \\ \dfrac{P_S}{\varepsilon_0\gamma\varepsilon_g} \dfrac{v\tau}{a + v\tau} \ln\left(\dfrac{v\tau}{a}\right)\dfrac{2H}{\pi(v\tau - a)}, & H \ll \{a, v\tau\}. \end{cases} \tag{21}$$

From Eq. (21) we derive two-point Pade approximations for $E_{\rm dm}$ quantitatively reproducing the behavior of exact expressions in the entire region of parameters,

$$E_{\rm dm} \approx \frac{P_S}{\varepsilon_0(\varepsilon_{33}^f + \gamma\varepsilon_g)} \frac{v\tau}{(a + v\tau)} \times \left\{1 + \frac{\pi\gamma\varepsilon_g}{2(\varepsilon_{33}^f + \gamma\varepsilon_g)}\left[\ln\left(\frac{a}{v\tau}\right)\right]^{-1}\frac{a - v\tau}{H}\right\}^{-1}. \tag{22}$$

Comparison of approximate expressions (22) with exact series (20) is shown in Fig. 4(a). The remarkable consequence of Eq. (20) is that at the wall-surface junction, the internal field $E_{\rm dm}$ decreases with domain wall velocity increase.

Note that the derived dependence of field on wall velocity is at first glance unphysical, since the length of "tail" of uncompensated charge moving after the wall increases with velocity increase. However, with the increase in tail length (about $v\tau$) the electric field at $z > 0$ tends to zero (similarly to the vanishing of the electric field outside the flat capacitor).[42] Thus, the damping role of the internal field at the surface $z = 0$ may be negligible for rapidly moving walls. In other words, there is a crossover between (I) polarization screening by low-mobility charges $\sigma(x,t)$ and (II) polarization screening by electrode free charges with giant (in theory infinite) mobility, which appeared when the sluggish charges are belated. Below, we demonstrate the "local" effect on the domain wall velocity v.

Equation (18) for the domain wall velocity could be solved either numerically and graphically for expressions (19), (20a), and (20b) or analytically using approximation (22), since the solution of cubic algebraic equations are available. Obtained results are presented in Fig. 4(b).

Note that at small values of external field the slope of the velocity dependence is from several times to several orders of magnitude smaller than at high fields (initial or ideal mobility). The dotted parts of curves correspond to the unstable regime when the velocity decreases with the field increase. The result means possible self-acceleration of the wall near the top surface, while the effect should become negligibly small with an increasing depth z.

Given that the field strength is maximal at the wall-surface junction and decreases with the depth increase (see curves 1–3 in Fig. 3), this depth dependence is expected to lead to the domain wall bending near the surface. This effect will be compensated by the depolarization field, and the interplay between the two will yield the equilibrium domain wall geometry. Rigorous self-consistent treatment of the problem is absent to date. Following Drougard and Landauer,[33] below we averaged the field over the domain wall surface in thin film.

V. DOMAIN WALL MOTION CAUSED BY THE EFFECTIVE FIELD AVERAGED OVER THE WALL SURFACE

For the films at small thickness (in comparison with the length of nucleus or rather small external field) internal field $E_{\rm dm}(z)$ should be averaged over the domain wall surface as given by Eq. (17). Then the effective value $\langle E_{\rm dm}(z)\rangle$ should determine the domain wall velocity (18).

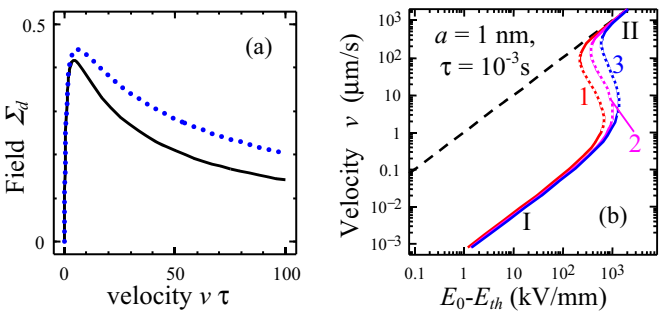

FIG. 4. (Color online) (a) The dependence of the normalized depolarization field $\Sigma_d = \varepsilon_0\varepsilon_{33}^f E_{\rm dm}/P_S$ at the wall-surface junction on the domain wall velocity $v\tau$ for $\gamma\varepsilon_g/\varepsilon_{33}^f = 0.5$ and $H = 5a$. Solid curves are series (20) and dashed curve is calculated from the approximate expressions (22). (b) Dependence of the domain wall velocity on the applied electric field for $\mu = 10^{-6}$ mm^2/(V s), $P_S = 0.75$ C/m^2, $\varepsilon_{33}^f = 30$, $\gamma\varepsilon_g/\varepsilon_{33}^f = 0.5$, and $\tau = 10^{-3}$ s; $a = 1$ nm. Solid curves 1, 2, and 3 correspond to the $H = 1$, 3, and 10 nm, dashed curve for $H = 0$ corresponds to the case without delay in screening. I and II designate two different screening regimes separated by the unstable region (dotted parts of the curves).

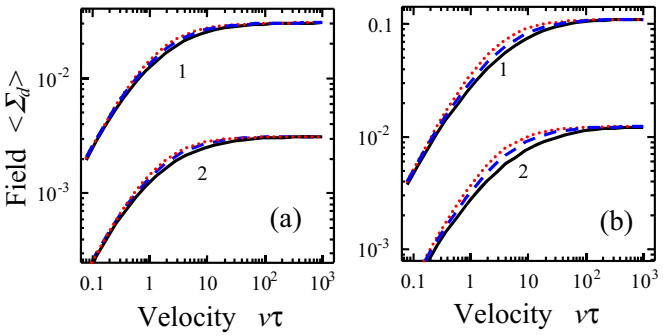

FIG. 5. (Color online) Dependence of effective field $\langle\Sigma_d\rangle = \varepsilon_0\varepsilon_{33}^f\langle E_{\rm dm}\rangle/P_S$ on the wall velocity for $H=5a$ and $\gamma\varepsilon_g/\varepsilon_{33}=0.8$ and 0.2 (panels a and b). Curves 1 and 2 correspond to $L/H=40$ and 400. Solid, dashed, and dotted curves correspond to exact (17), approximate (23), and Pade approximation (24).

Although the expansion in images series is available for the integral (17), the convergence of this series is very slowly due to the multiple reflections in three planes (two electrodes and interface between ferroelectric and dead layer). The approximate dependence of $\langle E_{\rm dm}(z)\rangle$ on the domain wall velocity v was obtained

$$\langle E_{\rm dm}(z)\rangle \approx \frac{P_S}{\varepsilon_0}\frac{2Hv\tau[f(v\tau,H,L)-f(a,H,L)]}{\pi[(v\tau)^2-a^2]},$$

$$f(q,H,L) = q^2\arccos\left[\frac{HL(\kappa_f+\varepsilon_g)}{q(\varepsilon_{33}^f H+\varepsilon_g L)}\right][q^2(\varepsilon_{33}^f H+\varepsilon_g L)^2 - (HL)^2(\kappa_f+\varepsilon_g)^2]^{-1/2}. \quad (23)$$

Here, the effective dielectric permittivity is introduced as $\kappa_f=\sqrt{\varepsilon_{11}^f\varepsilon_{33}^f}$. Corresponding Pade approximation of [1/1] type on variable $v\tau$ for Eq. (23) is derived as

$$\langle E_{\rm dm}(z)\rangle \approx \frac{P_S H}{\varepsilon_0(\varepsilon_{33}^f H+\varepsilon_g L)}\frac{2\arccos(\beta)v\tau}{[\pi\sqrt{1-\beta^2}a+2\arccos(\beta)v\tau]}, \quad (24a)$$

where β is introduced as

$$\beta = \frac{HL(\kappa_f+\varepsilon_g)}{a(\varepsilon_{33}^f H+\varepsilon_g L)}. \quad (24b)$$

Note that both approximations (23) and (24) reproduce the exact value of field in the limit of very high speed, namely, $\langle E_{d0}(z)\rangle \underset{v\tau\to\infty}{\to} P_S H/(\varepsilon_0\varepsilon_{33}^f H+\varepsilon_0\varepsilon_g L)$.

Comparison of the integral expression (17) for the averaged field $\langle E_{\rm dm}(z)\rangle$ with approximations (23) and (24) is shown in Fig. 5. The maximal difference between approximate and exact solutions does not exceed 30%, while they almost coincide at high and low values of $v\tau$. It appears that the difference could be even smaller for smaller values of L and for higher values of a. The dependence of averaged field $\langle E_{\rm dm}(z)\rangle$ on the domain wall velocity for different values of film thickness is presented in Fig. 6. In contrast to the maximal field $E_{\rm dm}(0)$, the effective field $\langle E_{\rm dm}(z)\rangle$ always increases with with the increase of domain wall velocity [compare Fig. 4(a) with Figs. 5 and 6]. As a result, the domain wall motion caused by the effective field averaged over the wall surface is always stable.

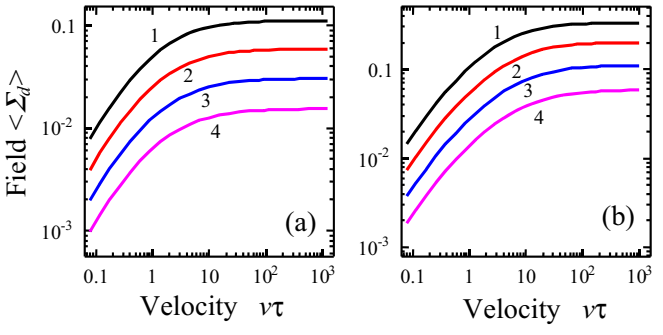

FIG. 6. (Color online) Dependence of the effective field $\langle\Sigma_d\rangle = \varepsilon_0\varepsilon_{33}^f\langle E_{\rm dm}\rangle/P_S$ on the wall velocity for $H=5a$ and $\gamma\varepsilon_\gamma/\varepsilon_{33}=0.8$ and 0.2 (panels a and b). Curves 1, 2, 3, and 4 correspond to $L/H=10$, 20, 40, and 80.

The influence of the effective field $\langle E_{\rm dm}(z)\rangle$ can be understood as follows. Using the simplest model one can easily see that linear dependence of internal field on velocity for its smaller values leads to the essential decrease in mobility, while the saturation of internal field at higher velocity could change threshold field but could not change mobility. It is seen from Fig. 7 that the slope of the curves is the same at higher field, while linear extrapolation to zero velocity gives different threshold value dependent on film thickness.

Physically, Fig. 7 [similarly to Fig. 4(b)] demonstrates the crossover between two screening regimes: regime (I) for low

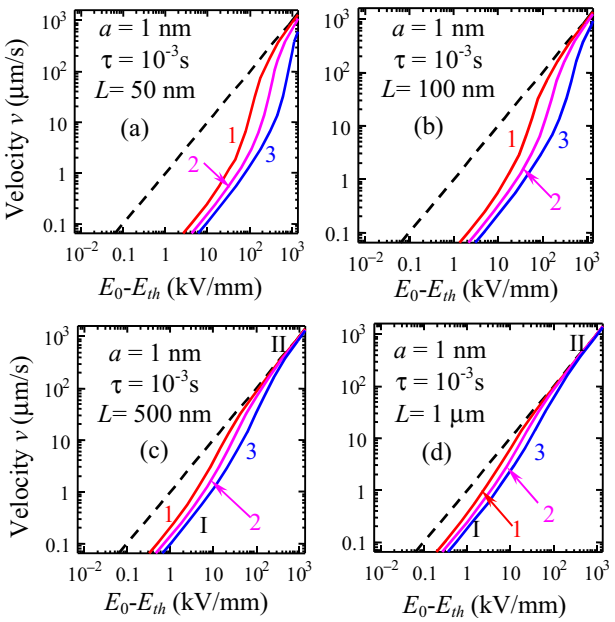

FIG. 7. (Color online) Dependence of the domain wall velocity on the applied electric field for $\mu=10^{-6}$ mm^2/(V s), $P_S=0.75$ C/m^2, $\varepsilon_{33}^f=30$, $\gamma\varepsilon_g/\varepsilon_{33}^f=0.5$, $\tau=10^{-3}$ s, $a=1$ nm, (a) $L=50$, (b) 100, and (c) 500 nm, and (d) 1 μm. Dashed curve is related to the ideal case without delay of screening (either $H=0$ or $\tau=0$); solid curves 1, 2, and 3 correspond to $H=1$, 3, and 10 nm. I and II designate two different screening regimes separated by the transient region.

domain wall velocity, when the wall can drag the sluggish screening charges σ, and regime (II) for high domain wall velocity, when the delay of sluggish screening charges are essential and the wall depolarization field is screened by the electrode free charges separated from the bound charges by the dead layer.

VI. SUMMARY

Here we analyzed the effect of the domain wall intrinsic width, screening relaxation time, and the dead layer thickness on the velocity of the 180°-domain wall *uniformly* moving under homogeneous external electric field in ferroelectric capacitor placed between the planar electrodes. We derived corresponding integral and approximate analytical expressions for electric field and algebraic equation for the domain wall velocity.

We demonstrate the crossover between two screening regimes: the first one corresponds to the low domain wall velocity, when the wall drags the sluggish screening charges, while the second regime appeared for high domain wall velocity, when the delay of sluggish screening charges are essential and the wall depolarization field is screened by the instant free charges located at the electrode.

The "local" motion at the wall-surface junction can be unstable for nonzero dead layer thickness, since the internal field at the wall-surface junction decreases with an increased domain wall velocity. The instability may lead to the domain wall-surface bending and actual broadening in thick samples. Finally, for thin films the averaging of the internal field can be performed over the film thickness. The motion caused by the effective field averaged over the domain wall surface is always stable. For thick samples the averaging should be performed over the nucleus volume. The latter is unknown and its shape should be calculated self-consistently.

ACKNOWLEDGMENTS

E.E.A., A.N.M., G.S.S., E.L.R., E.I.S., and V.Y.S. gratefully acknowledge financial support from National Academy of Science of Ukraine and Russian Academy of Science, joint Russian-Ukrainian grant under Grant No. NASU N 17-Ukr_a (RFBR under Grant No. N 08-02-90434). The research is supported in part (S.V.K.) by the Division of Scientific User Facilities, DOE BES.

APPENDIX

1. Phenomenological equation for the evolution of the screening charge $\sigma(x,t)$

Here we derive the phenomenological equation for the evolution of the screening charge $\sigma(x,t)$. For typical proper ferroelectrics semiconductors the thickness h of the screening layer is discussed in Ref. 43. Inside the ultrathin surface layer $0<z<h$ the continuity equation $\partial\rho_f/\partial t+\mathrm{div}\,\mathbf{j}_c=0$ (where $\mathbf{j}_c$ is electric current of the free carriers and ρ_f is the charge density of the free carriers) and Maxwellian equation $\mathrm{div}(\mathbf{P}_0+\varepsilon_0\hat{\varepsilon}^f_{ij}\mathbf{E}_f)=\rho_f$ are valid. Electric current $\mathbf{j}_c$ is assumed to be dominated by conductivity current $\mathbf{j}_c=\lambda\mathbf{E}_f$ (where λ is conductivity), while diffusion current can be neglected. Under the condition $\varepsilon^f_{11}=\varepsilon^f_{22}=\varepsilon^f_{33}$, this yields $\mathrm{div}\,\mathbf{j}_c=\lambda\,\mathrm{div}\,\mathbf{E}_f=\frac{\lambda}{\varepsilon_0\varepsilon^f_{33}}(\rho_f-\mathrm{div}\,\mathbf{P}_0)$. Substituting the expression into the continuity equation, we derived $\frac{\partial\rho_f}{\partial t}=\frac{\lambda}{\varepsilon_0\varepsilon^f_{33}}(\mathrm{div}\,\mathbf{P}_0-\rho_f)$ for $0<z<h$. Using the steplike approximation for the polarization $\mathbf{P}_0=\mathbf{P}_0(x,t)\theta(z)\theta(L-z)$ [where $\theta(z)$ is a Heaviside step function], integration of the equation over coordinate z in the region $0\le z\le h$ reduces to Eq. (8) for the surface charge density $\sigma=h\rho_f$ in the limiting case $h\to 0$.

2. Internal field distribution

Introducing the potential φ of quasistationary electric field $\mathbf{E}_{g,f}(x,z,t)=-\nabla\varphi_{g,f}(x,z,t)$ and assuming that the screening free charge is located inside thin layer at the boundary between dead layer and ferroelectrics while the spontaneous polarization is z independent, one can write the equations for potential distribution as follows:

$$\left(\frac{\partial^2}{\partial z^2}+\frac{\partial^2}{\partial x^2}\right)\varphi_g=0,\quad \text{for}\quad -H<z<0, \tag{A1a}$$

$$\left(\varepsilon^f_{33}\frac{\partial^2}{\partial z^2}+\varepsilon^f_{11}\frac{\partial^2}{\partial x^2}\right)\varphi_f=0,\quad \text{for}\quad 0<z<L. \tag{A1b}$$

Equation (A1) should be supplemented with the boundary conditions of fixed top and bottom electrode potentials, continuous potential, and normal component of displacement on the boundaries between dead layer and ferroelectric, namely,

$$\varphi_g(z=-H)=0,\quad \varphi_g(z=0)=\varphi_f(z=0),\quad \varphi_f(z=L)=0, \tag{A2a}$$

$$-\varepsilon^f_{33}\frac{\partial\varphi_f(z=0)}{\partial z}+\frac{P_{0n}(z=0)-\sigma}{\varepsilon_0}=-\varepsilon_g\frac{\partial\varphi_g(z=0)}{\partial z}. \tag{A2b}$$

Here σ is the effective surface density of the screening charges.

Using Fourier transformation $\varphi_{g,f}(x,z,t)=(2\pi)^{-1/2}\int_{-\infty}^{+\infty}\exp(-ik_1x)\tilde{\varphi}_{g,f}(k_1,z,t)dk_1$, one can rewrite Eq. (A1) as follows:

$$\left(\frac{\partial^2}{\partial z^2}-k^2\right)\tilde{\varphi}_g=0,\quad \text{for}\quad -H<z<0, \tag{A3a}$$

$$\left(\frac{\partial^2}{\partial z^2}-\frac{k^2}{\gamma^2}\right)\tilde{\varphi}_f=0,\quad \text{for}\quad 0<z<L. \tag{A3b}$$

Here $\gamma=\sqrt{\varepsilon^f_{33}/\varepsilon^f_{11}}$ is the dielectric anisotropy factor $k=|k_1|$. Since boundary conditions (A2) are linear on potentials and the coefficients do not depend on x, boundary conditions for $\tilde{\varphi}_{g,f}(k_1,z,t)$ can be obtained from Eq. (A2) by simple substitution of functions on x by their Fourier images. General solution of Eq. (A3) consists of the sum of exponential functions $\tilde{\varphi}_g(k,z,t)\sim\exp(\pm kz)$ and $\tilde{\varphi}_f(k,z,t)\sim\exp(\pm kz/\gamma)$. Using the conditions of short circuit ($U=0$), one can write

$$\tilde{\varphi}_g(k_1,z,t) = C_g(k_1,t)\sinh[k(z+H)],$$

$$\tilde{\varphi}_f(k_1,z,t) = C_f(k_1,t)\sinh\left[\frac{k(L-z)}{\gamma}\right]. \tag{A4}$$

Unknown functions $C_{g,f}$ should be determined from the other boundary conditions (A2). Namely, applying the conditions of potential and normal components continuity on the boundary between the dead layer and ferroelectric, one can write the following system of equations for $C_{g,f}$:

$$C_g \sinh(kH) = C_f \sinh\left(\frac{kL}{\gamma}\right), \tag{A5}$$

$$\varepsilon_{33}^f C_f \frac{k}{\gamma}\cosh\left(\frac{k}{\gamma}L\right) + \frac{\tilde{P}_0(k_1,t) - \tilde{\sigma}(k_1,t)}{\varepsilon_0} = -\varepsilon_g C_g k \cosh(kH). \tag{A6}$$

The solution of this system has the form

$$C_f = -\frac{\tilde{P}_0(k_1,t) - \tilde{\sigma}(k_1,t)}{\varepsilon_0}\frac{\sinh(kH)}{\frac{k}{\gamma}\varepsilon_{33}^f \cosh\left(\frac{k}{\gamma}L\right)\sinh(kH) + k\varepsilon_g \cosh(kH)\sinh\left(\frac{k}{\gamma}L\right)}. \tag{A7}$$

The normal component of electric field inside ferroelectric $\tilde{E}_{f3}(k_1,z,t) = -\partial\tilde{\varphi}_f(k_1,z,t)/\partial z$ is

$$\tilde{E}_{f3}(k_1,z,t) = -\frac{\tilde{P}_0(k_1,t) - \tilde{\sigma}(k_1,t)}{\varepsilon_0\gamma}\frac{\sinh(kH)\cosh\left[\frac{k}{\gamma}(L-z)\right]}{\frac{\varepsilon_{33}^f}{\gamma}\cosh\left(\frac{k}{\gamma}L\right)\sinh(kH) + \varepsilon_g \cosh(kH)\sinh\left(\frac{k}{\gamma}L\right)}. \tag{A8}$$

Near the surface $z \ll L$ of thick ferroelectric film ($L \gg H$),

$$\tilde{E}_{f3}(k_1,z,t) \approx -\frac{\tilde{P}_0(k_1,t) - \tilde{\sigma}(k_1,t)}{\varepsilon_0\gamma} \times \frac{\sinh(kH)\exp\left(-\frac{k}{\gamma}z\right)}{\frac{\varepsilon_{33}^f}{\gamma}\sinh(kH) + \varepsilon_g \cosh(kH)}. \tag{A9}$$

In Eq. (20) we introduced the following transcendental function:

$$F(z,a) = \frac{2}{\pi}\int_0^\infty dk \frac{a\exp(-kz)}{[1+(ka)^2]} = \cos\left(\frac{z}{a}\right) + \frac{2}{\pi}\left[\mathrm{Ci}\left(\frac{z}{a}\right)\sin\left(\frac{z}{a}\right) - \mathrm{Si}\left(\frac{z}{a}\right)\cos\left(\frac{z}{a}\right)\right] \approx \frac{2a}{2a+\pi z}, \tag{A10}$$

where $\mathrm{Si}(z)$ and $\mathrm{Ci}(z)$ are the sine and cosine integral functions.

*Corresponding author; morozo@i.com.ua
†Corresponding author; sergei2@ornl.gov

[1] B. Meyer and D. Vanderbilt, Phys. Rev. B **65**, 104111 (2002).
[2] R. Miller and G. Weinreich, Phys. Rev. **117**, 1460 (1960).
[3] Y.-H. Shin, I. Grinberg, I.-W. Chen, and A. M. Rappe, Nature (London) **449**, 881 (2007).
[4] Y. Ishibashi, J. Phys. Soc. Jpn. **46**, 1254 (1977).
[5] I. Suzuki and Y. Ishibashi, Ferroelectrics **64**, 181 (1985).
[6] T. J. Yang, V. Gopalan, P. J. Swart, and U. Mohideen, Phys. Rev. Lett. **82**, 4106 (1999).
[7] Q. Y. Qiu, V. Nagarajan, and S. P. Alpay, Phys. Rev. B **78**, 064117 (2008).
[8] I. Ponomareva, I. I. Naumov, I. Kornev, Huaxiang Fu, and L. Bellaiche, Phys. Rev. B **72**, 140102(R) (2005).
[9] L. Lahoche, I. Luk'yanchuk, and G. Pascoli, Integr. Ferroelectr. **99**, 60 (2008).
[10] S. V. Kalinin, C. Y. Johnson, and D. A. Bonnell, J. Appl. Phys. **91**, 3816 (2002).
[11] J. E. Spanier, A. M. Kolpak, J. J. Urban, I. Grinberg, L. Ouyang, W. S. Yun, A. M. Rappe, and H. Park, Nano Lett. **6**, 735 (2006).
[12] D. Li, M. H. Zhao, J. Garra, A. M. Kolpak, A. M. Rappe, D. A. Bonnell, and J. M. Vohs, Nature Mater. **7**, 473 (2008).
[13] Y. Watanabe, Phys. Rev. B **59**, 11257 (1999).
[14] M. Krcmar and C. L. Fu, Phys. Rev. B **68**, 115404 (2003).
[15] A. Rappe (unpublished).
[16] M. Stengel and N. A. Spaldin, Nature (London) **443**, 679 (2006).
[17] G. Gerra, A. K. Tagantsev, and N. Setter, Phys. Rev. Lett. **94**, 107602 (2005).

[18] G. Gerra, A. K. Tagantsev, N. Setter, and K. Parlinski, Phys. Rev. Lett. **96**, 107603 (2006).
[19] P. Aguado-Puente and J. Junquera, Phys. Rev. Lett. **100**, 177601 (2008).
[20] V. Ya. Shur, A. L. Gruverman, V. P. Kuminov, and N. A. Tonkachyova, Ferroelectrics **111**, 197 (1990).
[21] V. Ya. Shur, Ferroelectrics **340**, 3 (2006).
[22] V. Ya. Shur, E. L. Rumyantsev, A. G. Shur, A. I. Lobov, D. K. Kuznetsov, E. I. Shishkin, E. V. Nikolaeva, M. A. Dolbilov, P. S. Zelenovskiy, K. Gallo, and M. P. De Micheli, Ferroelectrics **354**, 145 (2007).
[23] M. A. Dolbilov, V. Ya. Shur, E. I. Shishkin, M. F. Sarmanova, E. V. Nikolaeva, S. Tascu, P. Baldi, and M. P. De Micheli, Ferroelectrics (to be published).
[24] E. V. Nikolaeva, V. Ya. Shur, M. A. Dolbilov, E. I. Shishkin, D. K. Kuznetsov, M. F. Sarmanova, O. A. Plaksin, and N. V. Gavrilov, Ferroelectrics (to be published).
[25] V. Ya. Shur, D. K. Kuznetsov, A. I. Lobov, E. V. Nikolaeva, M. A. Dolbilov, A. N. Orlov, and V. V. Osipov, Ferroelectrics **341**, 85 (2006).
[26] A. I. Lobov, V. Ya. Shur, D. K. Kuznetsov, S. A. Negashev, D. V. Pelegov, E. I. Shishkin, and P. S. Zelenovskiy, Ferroelectrics **373**, 99 (2008).
[27] R. Dittmann, R. Plonka, E. Vasco, N. A. Pertsev, J. Q. He, C. L. Jia, S. Hoffmann-Eifert, and R. Waser, Appl. Phys. Lett. **83**, 5011 (2003).
[28] I. B. Misirlioglu, A. L. Vasiliev, M. Aindow, S. P. Alpay, and R. Ramesh, Appl. Phys. Lett. **84**, 1742 (2004).
[29] S. P. Alpay, I. B. Misirlioglu, V. Nagarajan, and R. Ramesh, Appl. Phys. Lett. **85**, 2044 (2004).
[30] V. Nagarajan, C. L. Jia, H. Kohlstedt, R. Waser, I. B. Misirlioglu, S. P. Alpay, and R. Ramesh, Appl. Phys. Lett. **86**, 192910 (2005).
[31] M. Grossmann, O. Lohse, D. Bolten, U. Boettger, T. Schneller, and R. Waser, Appl. Phys. Lett. **80**, 1427 (2002).
[32] W. J. Merz, J. Appl. Phys. **27**, 938 (1956).
[33] M. E. Drougard and R. Landauer, J. Appl. Phys. **30**, 1663 (1959).
[34] D. R. Callaby, J. Appl. Phys. **36**, 2751 (1965).
[35] D. R. Callaby, J. Appl. Phys. **38**, 431 (1967).
[36] M. Grossmann, O. Lohse, D. Bolten, U. Boettger, and R. Waser, J. Appl. Phys. **92**, 2688 (2002).
[37] L. Pintilie and M. Alexe, J. Appl. Phys. **98**, 124103 (2005).
[38] I. B. Misirlioglu, M. Alexe, L. Pintilie, and D. Hesse, Appl. Phys. Lett. **91**, 022911 (2007).
[39] A. K. Tagantsev and G. Gerra, J. Appl. Phys. **100**, 051607 (2006).
[40] G. B. Stephenson and K. R. Elder, J. Appl. Phys. **100**, 051601 (2006).
[41] G. Catalan, H. Bea, S. Fusil, M. Bibes, P. Paruch, A. Barthelemy, and J. F. Scott, Phys. Rev. Lett. **100**, 027602 (2008).
[42] This behavior can be illustrated by considering a simple system consisting of the finite strip with width b and with constant surface charge placed at the distance H from the electrode. In the case the full field distribution can be obtained in the evident form. The field behaves as $\pi/2-\arctan[b/(2H)]$ at the film surface near the edge of the strip and vanishes with an increased b.
[43] V. M. Fridkin, *Ferroelectrics Semiconductors* (Consultants Bureau, New York, 1980).